ORIGINAL PAPER

Crystallization, morphology, optical properties, tear properties and antibacterial properties of nano zinc oxide composites

Ying Wang[1,2] · Li-Zhi Liu[1,2] · Chengcheng Tian[1,2] · Yuanxia Wang[2] · Lixin Song[2] · Ying Shi[2]

Abstract

Nanometer Zinc oxide (nano ZnO) composites are widely used in the packaging industry due to their excellent antibacterial properties. In this study, low-doped (0.2%) and high-antibacterial (99.9%, R = 6.9) nano ZnO composites with different matrices were prepared using a masterbatch blending method. To investigate the effect of different matrices on antibacterial properties, we decreased the solid content of nano ZnO to 0.05% and prepared antibacterial films by melt-blending with ethylene vinyl acetate copolymer (EVA), polyolefin elastomer (POE), linear low-density polyethylene (LLDPE), high-density polyethylene (HDPE), and amorphous polymer polycarbonate (PC). The results showed that low melt strength and high crystallinity would decrease the antibacterial activity of the composite. At room temperature, the PC with a frozen molecular chain can hinder the migration of small molecules, thereby reducing antibacterial activity. Polar ZnO is more compatible with polar vinyl acetate (VA), leading to the hindered surface migration of ZnO and reduced antibacterial activity. Most importantly, low crystallinity does not necessarily lead to a reduction in barrier properties. The dense and rich layered arrangement of polyolefin elastomer (POE) increases its ability to impede the migration of nano ZnO, thereby significantly reducing its antibacterial effectiveness. A concentration of 0.05% ZnO/linear low-density polyethylene (LLDPE) exhibited an antibacterial rate of up to 99.3%. Additionally, adding a small amount of nano ZnO improves the tear resistance of antibacterial composite materials. This study provides a theoretical basis for the preparation of low doping, high antibacterial and excellent comprehensive performance.

Keywords Nano ZnO · Nanocomposites · Antibacterial activity · Crystal structure

Introduction

Antibacterial packaging materials have the potential to enhance the safety and quality of food during processing, packaging, and transportation while reducing the incidence of food corruption [1, 2]. In recent years, nanometer zinc oxide (nano ZnO) materials have gained significant attention as antibacterial agents [3–7]. Their safety, long-lasting effect, heat resistance, and excellent antibacterial properties make them widely used in food and pharmaceutical packaging applications [8–11]. Compared with common silver-based

antibacterial agents, the antibacterial mechanism of ZnO is similar and mainly includes direct contact with proteins to destroy cells, Zn^{2+} ions leaching to disrupt cell permeability, and the production of active oxygen (ROS) to decompose nutrients [12–17]. Zinc-based antibacterial materials are broad-spectrum antibacterial substances that can inhibit multiple bacteria [18]. In comparison, the efficacy of silver-based antibacterial materials is higher, but their activity is limited to specific microorganisms and, therefore, not suitable for all fields [19]. Due to the higher efficacy of silver-based antibacterial materials, less silver is usually required to achieve the desired antibacterial effect [20]. In contrast, zinc-based antibacterial materials require a larger amount of zinc to achieve similar antibacterial effects [21]. However, zinc-based materials are more cost-effective than silver, so the use of zinc-based antibacterial materials can also have cost advantages. ZnO has broad antibacterial activity and lower costs. However, the study has shown that adding a higher concentration of nano ZnO to achieve satisfactory antibacterial effects leads to a

✉ Ying Shi
   shiying86@aliyun.com

1   School of materials science and engineering, Shenyang University of Technology, Shenyang 110142, China

2   Advanced Manufacturing Institute of Polymer Industry, Shenyang University of Chemical Technology, Shenyang 110142, China

decrease in the mechanical properties of composite materials [22]. Therefore, it is essential to prepare low-doped and highly antibacterial composite materials that have minimal impact on other properties.

On the other hand, Negi et al. [23] proposed that the concentration of ZnO affects its antibacterial activity, and the higher the migration rate of nano ZnO from the matrix, the better the antibacterial activity due to the ZnO antibacterial mechanisms. It is well known that crystallinity significantly affects barrier performance [24–26]. Hong-Biao and Chang-Ying [27] investigated the blocking ability of polypropylene (PP) with different crystallinity to nano ZnO migration. The results showed that higher crystallinity led to more limited ZnO migration. Interestingly, the antibacterial activity of composites prepared by adding the same amount of ZnO into various matrices has been found to be different. Alojz Anžlovar et al. [28] showed that the antibacterial efficiency of ZnO/ high-density polyethylene (HDPE) was greater than that of ZnO/PP under the same ZnO content in the composite. Studies on composite materials have demonstrated that when ZnO nanoparticles are dispersed in a polyamide (PA) matrix, they exhibit better dispersion and antibacterial properties compared to a low-density polyethylene (LDPE) matrix, depending on the PA matrix's ability to disperse in water [29]. However, the effects of interactions between different substrates and ZnO on antibacterial performance have not been elucidated. In summary, understanding the mechanism of the antibacterial action of nano ZnO in different matrices can help to prepare antibacterial materials with low doping and high antibacterial activity without adversely affecting other properties.

In this study, the melt blending method was employed to prepare five types of highly antibacterial nanocomposites. The fabricated composite films exhibited remarkable antibacterial performance while significantly reducing the nano ZnO content compared to previous literature. Meanwhile, they minimized adverse effects on optical properties and improved mechanical performance. Furthermore, we investigated the influence of material microstructure, including crystallinity, layered stacking structure, and molecular chain fluidity, on the dispersion of inorganic particles within the polymer matrix. The main factors contributing to the variations in antibacterial performance among the five composite materials were elucidated by combining insights into antibacterial mechanisms. This study provides a solid theoretical foundation for matrix selection and offers practical strategies for developing commercially viable antibacterial products.

Experimental section

Materials

Commercial high-density polyethylene (HDPE) TR144 and linear low-density polyethylene (LLDPE) 7042 N

Table 1 Melt index (MI) of the materials used

Sample	MI (g/10 min)	Melting index test conditions
EVA	75.00	2.16 kg, 190 °C
POE	1.01	2.16 kg, 190 °C
LLDPE	2.07	2.16 kg, 190 °C
HDPE	0.18	2.16 kg, 190 °C
PC	6.70	1.2 kg, 300 °C

(China Petroleum & Chemical Co., Maoming, China), ethylene-octene copolymer (POE) ENGAGE 8480 (Dow Chemical Company, America), ethylene-vinyl acetate copolymer (EVA) 530 (Nipoflex® Tosoh Corporation, Japan), and polycarbonate (PC) L-1250Y (Teijin Corporation, Japan) were used in this experiment. Nano ZnO ethanol solution (ZnO solid content, 20%) was obtained from Xuancheng Jingrui New Material Co., Ltd (Anhui, China). The particle size of nano ZnO is 15 nm. POE is an ethylene-octene copolymer with a 20 wt% octene content, and EVA is an ethylene-vinyl acetate copolymer with a 6 wt% vinyl acetate content. Table 1 lists the melt index (MI) and melting index test conditions for each material.

Preparation of the antibacterial resin and films

We prepared antibacterial composites with 0.05% and 0.2% nano ZnO content using the masterbatch blending technique and a twin-screw extruder (TDS-20B, Nanjing Norda Extrusion Equipment Co., Ltd, Nanjing, China). We first prepared masterbatches of several substrates with nano ZnO content of 4% before adding them to the matrix in proportion for melt blending. This process was repeated three times to obtain nano ZnO antibacterial material with uniform dispersion. The processing temperature of each sample is presented in Table 2. The solid content of nano ZnO composite materials without any concentration labeling in this article is 0.05%.

We used a plate vulcanizer (Qingdao Yadong Rubber Machinery Co., Ltd., China) to press the samples for 5 min under a certain pressure (5 MPa) and processing temperature, followed by rapid cooling to room temperature. The resulting

Table 2 Processing conditions of nano ZnO composites

Sample	ZnO/EVA	ZnO/POE	ZnO/ LLDPE	ZnO/ HDPE	ZnO/PC
Processing temperature (°C)	160	180	180	180	250

film was used for the characterization of antibacterial activity, light transmittance, and tear resistance. We also prepared 1 mm thick sheets using a steel mold for small-angle X-ray diffraction characterization.

Small Angle X-ray Scattering (SAXS)

Small angle X-ray scattering (SAXS) measurements were performed at the Beijing 1W2A Beamline using a wavelength (λ) of 0.1542 nm (Cu K α). The scattering intensity was detected using a 1024×1024 pixels detector (MAR165CCD), with the distance between the sample and the detector set at 1665.56 mm. The exposure time was 15 s.

Mass flow rate test

The melt index was determined following GB/T3682.1-2018. The test temperatures were set at the processing temperature of each material, with a load of 2.16 kg.

Measurement of the antibacterial activity on plastics surface

We characterized the antibacterial rate (AR) of the nano ZnO composites against *Escherichia coli* (*E. coli*) (ATCC8739) using the GB/T31402-2015 method. The AR and antibacterial performance value (R) were evaluated by GB/T31402-2015 and GB21551.2-2010.

Thermal analysis

The melting and crystallization behavior of the samples were characterized using a DSC 3 (Mettler Toledo) differential scanning calorimeter in a nitrogen atmosphere. The ethylene series samples were heated to 200 ℃, cooled to -20 °C, and then heated up again to 200 °C at a temperature rate of 10 ℃/min to evaluate the crystallization temperature (T_c), melting temperature (T_m), and enthalpy of melting (ΔH_m). In this experiment, the glass transition temperature (T_g) of PC was also evaluated. The normalized crystallinity (X_c) of the polyethylene (PE) component was determined using the following equation [30]:

$$X_c(\%) = \Delta H_m / \phi \Delta H_m^0 \tag{1}$$

where φ is the weight fraction of PE in the copolymer, and the theoretical melting heat ΔH_m^0 of 100% crystalline PE is 293 J/g [31].

Thermogravimetric analysis (TGA)

TGA was conducted in a TG instrument thermal analyser (STA449C, Netzsch, Germany). The sample was heated from 50 to 600 °C or 800 °C at the rate of 10 °C/min in N_2 atmosphere.

Oxygen transmission rate

To measure the gas permeability of plastic film, a Gas Permeability Tester (GTR-701R, SYSTESTER, China) was used under standardized conditions of 25 °C, 101 kPa pressure, and 50% RH humidity according to GB/T 1038. The POE and LLDPE films, measuring an area of 36 cm^2, were placed into the test cell and subjected to vacuum conditions on one side while pure oxygen flowed in from the other.

Scanning Electron Microscope (SEM)

The surface morphology of the composite material was analyzed using the scanning electron microscope (FE-SEM JSM-7500 F, JEOL Ltd., Japan). The surface was coated with gold and observed under SEM at an accelerating voltage of 5 kV with a magnification of 20,000 times.

Small angle light scattering

A small-angle laser scattering instrument was constructed in-house to investigate the shape and size of spherulites. The experimental setup comprises five main components: a laser transmitter (Compass 315 M-50, Beijing Laser wave Photoelectric Technology Co., Ltd) with a laser wavelength (λ) of 520 nm, a polarizer, a rotating sample stage, another polarizer, and a receiving white screen. The average radius (R) of the spherulites can be computed utilizing the following formula [32]:

$$D = 4.09/4\pi\sin\frac{m}{2} \tag{2}$$

The distance (D) between the sample and the image-receiving screen was 5.5 cm. The ratio of the distance from the center of the pattern to the brightest point of the four lobes (L) to the vertical distance of the sample to the paper acceptor screen (D) represents the tangent of the scattering angle θ_m.

Haze and light transmittance test

The sample was tested in accordance with national standard GB/T 2410 − 2008, using the TH-100 light transmittance/haze tester from Hangzhou Caipu Technology Co., Ltd. To prepare the sample for testing, the film was flattened, and a small amount of liquid paraffin was evenly applied to both sides of the film, which was smoothed out. The haze that was measured after applying liquid paraffin to the sample is known as the internal haze.

The tear resistance test

The tear resistance test was conducted using a universal tensile testing machine (Instron 3365, Boston, MA, USA) per the standard method QBT1130-1991. A right-angle tear spline was torn at a separation speed of 200 mm/min. The experiment was repeated five times, and the average value was recorded.

Result and discussion

Size and dispersibility of the nano ZnO in the PC matrix

In Fig. 1(a), the SAXS curve of ZnO/PC (0.2%) displays high scattering intensity near the beamstop, which is attributed to scattering from the nano ZnO particles in a very dilute system [33].

Figure 1(b) illustrates the Guinier curve alongside the linear fitting curve. The average size of the nano ZnO particles was quantitatively calculated using the Guinier scattering theory based on the scattering of particles in the system. The Guinier equation is given as follows [34]:

$$I_{(q)} = I_e N n^2 exp\left(-\frac{q^2 R_g^2}{3}\right) \qquad (3)$$

In the equation, I_e represents the scattering intensity of electrons, N denotes the relative number of scatterers, n represents the number of electrons per individual particle, and R_g stands for the radius of gyration. q represents the scattering vector, which is calculated as [35]:

$$q = 4\pi \, sin \, \theta / \lambda \qquad (4)$$

where λ is the X-ray wavelength (0.154 nm), and θ is half the scattering angle (2θ). The formula (3) expressed in logarithmic form with base e is obtained as follows:

$$ln \, I = ln \, I_e n^2 N - \frac{R_g^2}{3} q^2 \qquad (5)$$

Since I_e, n, and N are constants in the scattering system, I_0 is defined as:

$$I_0 = I_e n^2 N \qquad (6)$$

Formula (3) can be transformed as follows:

$$ln \, I = ln \, I_0 - \frac{R_g^2}{3} q^2 \qquad (7)$$

Plot the lnI-q^2 graph. By performing a linear fit on the graph, the slope can be used to determine the radius of the gyration (R_g) of the scattering system. Nano ZnO particles are spherical, and therefore, the particle size (r) in the PC matrix is defined as [36]:

$$R_g = \sqrt{\frac{3}{5}} r \qquad (8)$$

The estimated particle size of nano ZnO in the PC matrix was 15.1 nm, which is very close to the average particle size of the purchased nano ZnO. This result indicates that the nano ZnO is almost monodisperse in the PC matrix, with a narrow particle size distribution, uniform dispersion, and no apparent agglomeration.

Antibacterial activity of ZnO composites (0.2%) toward *E. coli*

The anti-*E. coli* activity of nano ZnO antibacterial composite materials was characterized by the standard method, GB/T31402-2015. Table 3 shows that the antibacterial rate of the five types of nano ZnO composites, with a 0.2% nano ZnO content, was 99.9%, and R was 6.9. According to GB21551.2-2010, an antibacterial rate of $\geq 90\%$ indicates an antibacterial effect. Therefore, these five composites can achieve a high antibacterial rate. In contrast, the antibacterial rate of ZnO/HDPE film (with a ZnO content of 1%) prepared by Li and Li [22] was only 98.4%. These low-doped nano ZnO antibacterial materials exhibit high antibacterial activity due to the excellent dispersion of nano ZnO found in Sect. 2.1. To investigate the influence of different matrices on the antibacterial activity of nanocomposite materials, the content of nano ZnO in the antibacterial composite material was reduced by four times to 0.05%.
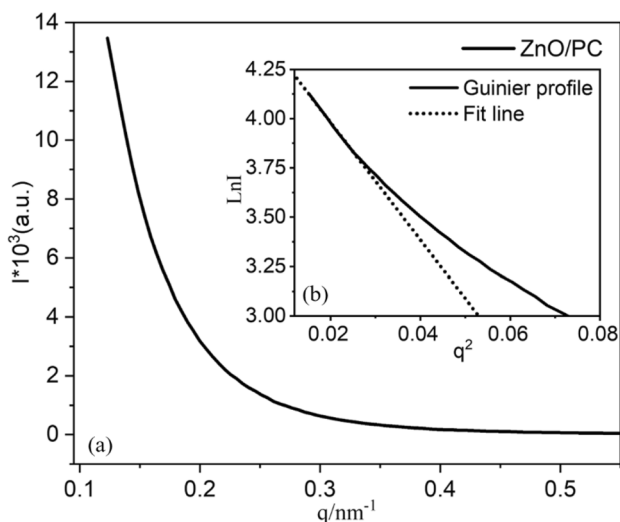

Fig. 1 Linear SAXS (**a**) and Guinier profiles (**b**) of ZnO/PC

Table 3 Antibacterial rate and the R of nano ZnO blends

Sample	Antibacterial rate(%)	R
ZnO/EVA (0.2%)	99.9	6.9
ZnO/POE (0.2%)	99.9	6.9
ZnO/LLDPE (0.2%)	99.9	6.9
ZnO/HDPE (0.2%)	99.9	6.9
ZnO/PC (0.2%)	99.9	6.9

2.3 Melt Index and antibacterial results analysis

Melt index and antibacterial results analysis

Table 4 shows the melt index of five pure materials under corresponding processing conditions. Comparing the melt index of five pure substances, EVA (22.36 g/10min) has the largest melt index, followed by PC (2.24 g/10min) and LLDPE (1.61 g/10min), and the melt index of POE and HDPE are relatively small (0.64 g/10min and 0.17 g/10min). For different substrates, the higher the melt index, the stronger the fluidity at the corresponding processing temperature. Therefore, EVA has better liquidity. The antibacterial test results of five nano ZnO composite films are shown in Table 5. The antibacterial rate of ZnO/LLDPE (99.3%) was higher than that of ZnO/EVA (95.3%), ZnO/POE (67.9%) and ZnO/PC (55.4%). The antibacterial rate of ZnO/HDPE (46.4%) was the lowest. From the data of melt index (Table 4), EVA has a high melt index (22.36 g/min) and strong fluidity, which is conducive to a more uniform dispersion of nano ZnO and a better antibacterial rate during processing. The melt indexes (0.64 g/10min, 1.61 g/10min, 0.17 g/10min and 2.24 g/10min) of POE, LLDPE, HDPE and PC have little difference, but their antibacterial rates differ significantly. The results show that the high melt strength of the material during processing has a positive but not the most critical effect on the antimicrobial properties of the final ZnO blend. Therefore, we cannot ignore the influence of the crystal structure of the matrix on the antibacterial properties.

Table 4 Melt index of four neat materials under processing temperature

Sample	MI (g/10min)	Processing temperature (°C)
EVA	22.36	160
POE	0.64	180
LLDPE	1.61	180
HDPE	0.17	180
PC	2.24	250

Table 5 Antibacterial rates of the nano ZnO composite films against *E. coli*

Sample	Antibacterial rate (%)	R
ZnO/EVA (0.05%)	95.2	1.3
ZnO/POE (0.05%)	67.9	0.4
ZnO/LLDPE (0.05%)	99.3	2.1
ZnO/HDPE (0.05%)	46.4	0.2
ZnO/PC (0.05%)	55.4	0.3

Melting and crystallization behavior of different polymers and corresponding nano ZnO Composites

Non-isothermal crystallization of semi-crystalline and amorphous polymers were analyzed using differential scanning calorimetry (DSC) through a heating, cooling, and reheating process. The results, including T_g, T_c, T_m, and X_c of Fig. 2, are presented in Table 6. Figure 2(a) illustrates the crystallization behavior of four ethylene series semi-crystalline polymers and amorphous polymer PC. During the cooling process, the T_c of ZnO/EVA composites shifted to a higher temperature than pure EVA, indicating that ZnO nanoparticles may serve as nucleation sites for heterogeneous nucleation, facilitating the growth of EVA molecular chains (with nanoparticles as the core) at elevated temperatures. Additionally, an increase in the crystallization temperature of ZnO blends was observed in cooling crystallization curves of POE and LLDPE, indicating that ZnO particles can induce crystallization in these materials. Among them, nano ZnO had the strongest ability to induce crystallization in EVA, followed by POE and LLDPE. This may be attributed to the hydrophilic characteristics of ZnO, while EVA contains vinyl acetate (6%), which is polar and hydrophilic. Therefore, the effect of EVA and ZnO is stronger. Notably, no significant change in T_c was observed in the cooling curves of the composites containing HDPE of ZnO, compared to EVA, POE, and LLDPE. This suggests that ZnO has a weak ability to induce crystallization in HDPE with regular molecular chain arrangement, possibly due to differences in their crystallization ability, as discussed further.

The thermograms obtained during the second heating process are shown in Fig. 2(b). As seen from this figure and Table 6, the melting peak of ZnO/POE composites moves to a lower temperature and the crystallinity is significantly increased compared to POE, indicating that ZnO/POE has more and smaller crystals than POE. In Table 6, the T_m of ZnO/EVA, ZnO/LLDPE, and ZnO/LLPE are slightly higher, and crystallinity are slightly lower than that of corresponding pure polyolefin, indicating that the crystals of these three composites are fewer and larger than those of pure materials. Notably, the T_g of the ZnO/PC composite is 140.2 °C, indicating that
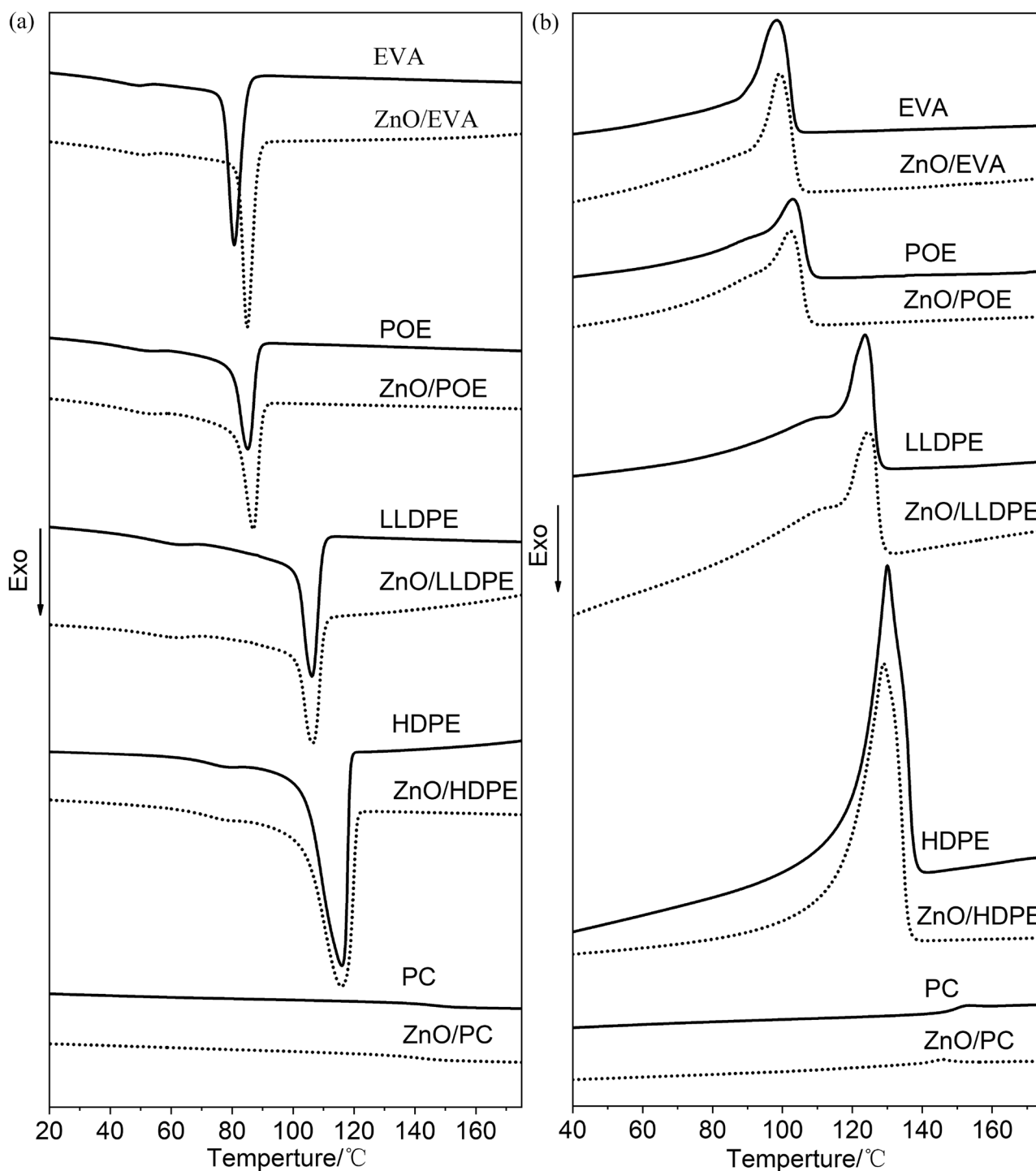
Fig. 2 DSC cooling curve (**a**) and heating curve (**b**) of different polymers and corresponding nano ZnO composites

the molecular chains of PC in ZnO/PC freeze at room temperature, making it difficult for small molecule nano ZnO to migrate from the PC. As indicated in Table 6, the antibacterial activity of PC is low (55.4%), which might be related to the reduced ability of ZnO to migrate to the surface. Similarly, the T_m of pure EVA and POE is

significantly lower than that of pure LLDPE and HDPE, indicating that the crystal size of EVA and POE is much smaller than that of LLDPE and HDPE. In Table 6, compared to the X_c of other polyolefins, HDPE exhibits the highest crystallinity in semi-crystalline polymers, denoting an evidently stronger crystallization ability. This may

Table 6 DSC data of five different polymers and corresponding nano ZnO composites

Sample	T_c (℃)	T_m (℃)	X_c (%)	T_g (℃)
EVA	81.18	98.21	28.89	----
ZnO/EVA	85.52	98.88	28.33	----
POE	85.53	103.28	32.47	----
ZnO/POE	87.26	101.90	37.75	----
LLDPE	106.36	123.34	38.01	----
ZnO/LLDPE	106.93	124.06	36.29	----
HDPE	116.95	129.16	58.08	----
ZnO/HDPE	116.60	128.40	57.42	----
PC	----	----	----	148.13
ZnO/PC	----	----	----	140.59

be attributed to the higher regularity of the main chain in HDPE than in LLDPE, whose main chain is a short branch chain with X_c of 38.01%. The crystallinity of POE and EVA is much lower than that of the two common ethylene polymers. Among them, the crystallinity of POE is 32.47%, which could be due to the intervention of octene (20%) in the molecular chain of elastomer POE, destroying the crystallization of polyethylene. The crystallinity of EVA is 28.89% because vinyl acetate (6%) inhibits ethylene crystallization. In Table 5, the antibacterial rates of ZnO/EVA, ZnO/POE, and ZnO/HDPE are 95.2%, 67.9%, and 46.4%, respectively. These results indicate that the ZnO/EVA composite offers the best inhibition against *E. coli*, whereas ZnO/HDPE is the least effective, and POE is moderately effective. For semi-crystalline polymers, nano ZnO cannot exist in the crystalline phase but exists in the amorphous phase and then migrates out of the sample surface [37, 38]. Materials with low crystallinity contain fewer crystals and have less ability to hinder the migration of ZnO [39]. Therefore, ZnO in composites with low crystallinity is easier to migrate to the surface and achieve higher antibacterial activity. Surprisingly, the crystallinity of LLDPE was significantly higher than that of EVA (38.01% vs. 28.89%), but the antibacterial rate of ZnO/EVA was slightly lower than that of ZnO/LLDPE (99.3% vs. 95.2%). This is because polar EVA is more likely to interact with polar ZnO, thereby impeding the migration of nano ZnO. Consequently, the antibacterial rate of ZnO/EVA is slightly lower than that of ZnO/LLDPE. The crystallinity of LLDPE is slightly higher than that of POE, but the antibacterial ability of ZnO/LLDPE is stronger than that of ZnO/POE because POE has smaller and more crystals than LLDPE. The tight arrangement of these crystals may hinder the migration of ZnO, which will be further verified in the subsequent discussion (Fig. 3).

The thermal degradation of nano ZnO composites

Figure 4 shows the TGA thermograms of polymer and nano ZnO composites. In Fig. 4(a), two weight loss steps are observed in the EVA group within the temperature ranges of 300–410 ℃ and 410–500 ℃. The first step is attributed to the degradation of the EVA copolymer, with the release of acetic acid at higher temperatures. The second step corresponds to the degradation of the ethylene main chain [40]. Only one degradation step related to the main chain is observed in the POE, LLDPE, HDPE, and PC groups. The addition of nano ZnO particles does not significantly affect the thermal degradation curves of EVA, POE, LLDPE, and HDPE, as the amount of nano ZnO added is relatively small and does not exert a pronounced catalytic effect on the main chain. However, for ZnO/PC, the thermal degradation temperature is advanced from 467.1 ℃ to 452.5 ℃ at a 5% weight loss, while the residue carbon content decreases from 22.8 to 20.2%. This can be attributed to the promotion of PC ester bond cleavage by the nano ZnO particles [41].

Effect of nano ZnO on the lamellar structure of semi-crystalline polymers

The linear SAXS profiles for four different polyolefins and ZnO composites at room temperature are presented in Fig. 4, where a scattering peak is observed at $q = 0.3$ nm^{-1} or 0.4 nm^{-1}, corresponding to the long period for polyolefin lamellar stacks. The scattering peak of ZnO composites is significantly higher than that of pure materials, and the peak deformation is wider, indicating that the electron cloud density difference of ZnO composites is larger and the crystalline order is lower. This is caused by the scattering of nano ZnO particles, as seen in the SAXS analysis of the PC group (Fig. 1).

Table 7 displays the averaged interlamellar distance (long period) (L) obtained from Gauss fitting of Lorentz-corrected (Iq^2-q) SAXS profiles (inset figures) and the lamellar size (Lc) obtained from the correlation function for these samples. The position of the peak q_{peak} is related to the long period (L) by Bragg's law [42] and formula (4).

$$L = 2\pi / q_{peak} \tag{9}$$

The average thickness of the crystalline phase (Lc) and amorphous phase (La) was calculated using the normalized one-dimensional correlation function K(z), which was evaluated from the scattered intensity I(q) with the following equation [43]:

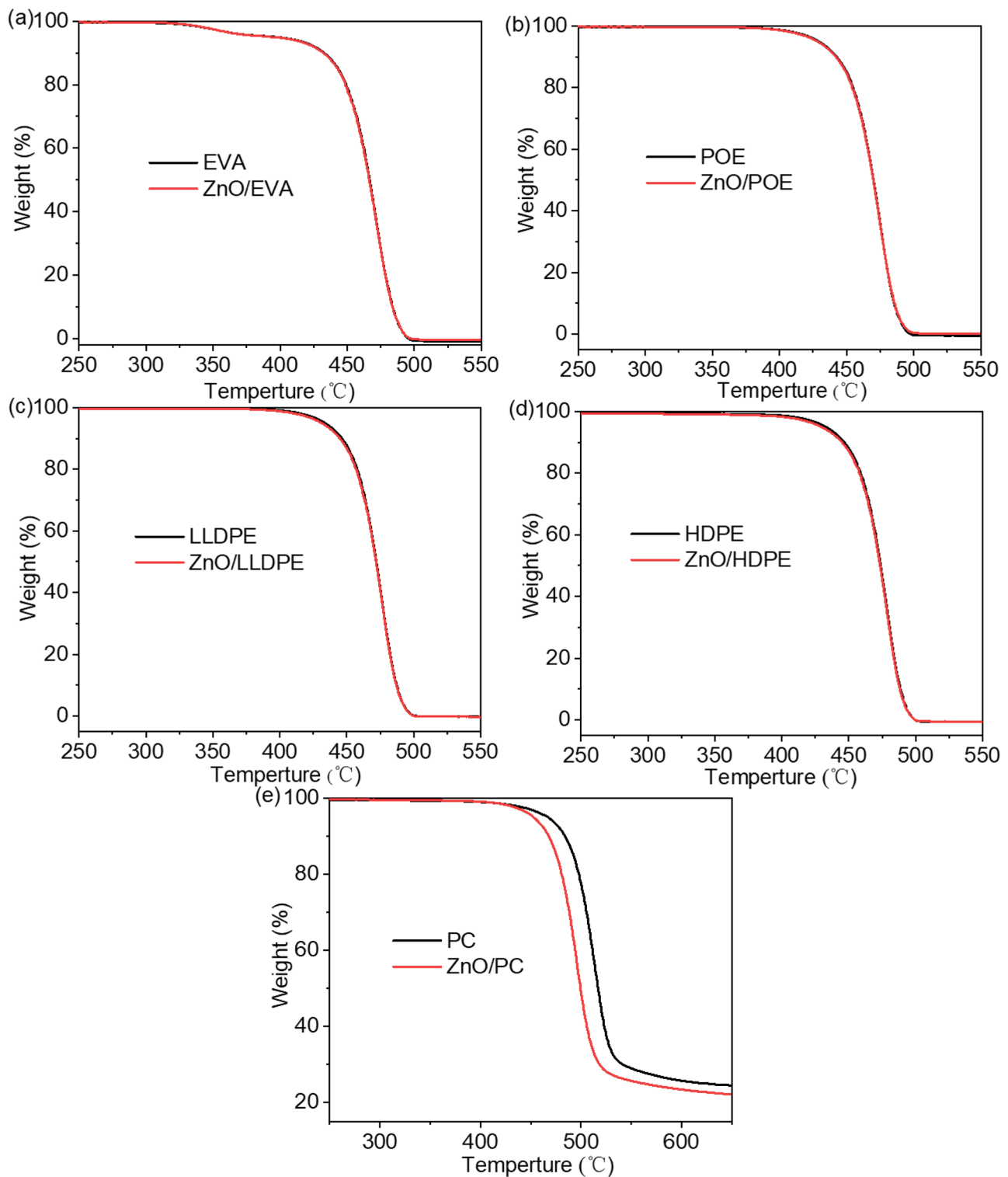$$K(z) = (1/K(0)) \int_0^\infty q^2 I(q) cos(qz) dq \tag{10}$$

Fig. 3 TG curves of (**a**) EVA group, (**b**) POE group, (**c**) LLDPE group, (**d**) HDPE group, (**e**) PC group

where I(q) is the scattering intensity, z is the correlation distance measured along the direction of the electron density distribution. The value on the z-axis at which the tangent line to the linear portion of the K(z)-z curve intersects with the first minimum (trough) horizontal line is denoted as Lc. La is the value obtained by subtracting Lc from L. As indicated in Table 7, the La of semi-crystalline polymer samples is smaller than the particle diameter of nano ZnO (15 nm),
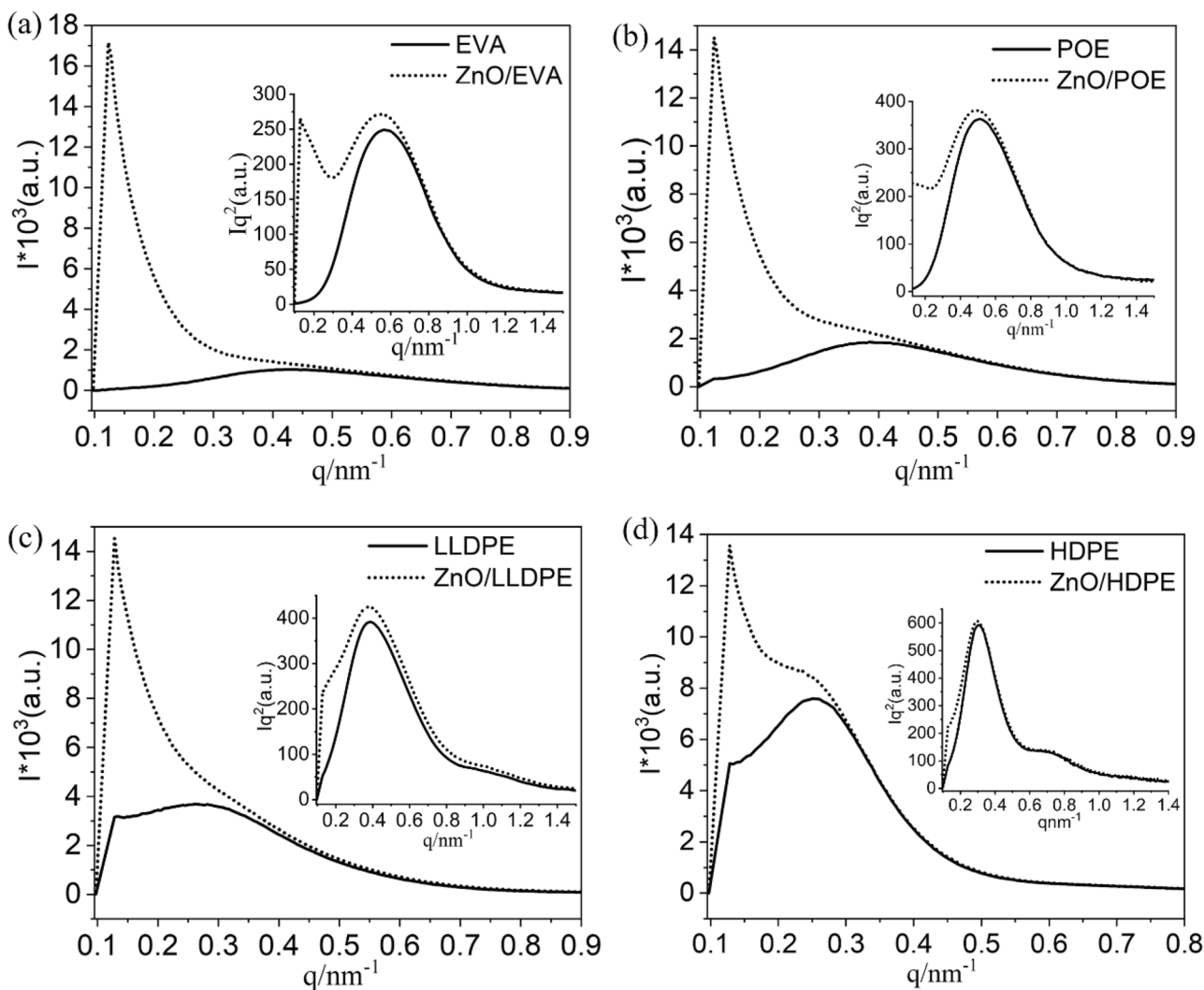
Fig. 4 Linear and Lorentz-corrected SAXS profiles of different materials. (**a**) EVA and ZnO/EVA (**b**) POE and ZnO/POE (**c**) LLDPE and ZnO/LLDPE (**d**) HDPE and ZnO/HDPE

suggesting that nano ZnO cannot penetrate the amorphous region between the lamellae. The insignificant variation in the long period of the nano ZnO composites can be attributed

Table 7 The results of long period (L), lamellar size (Lc) and amorphous region size (La)

Sample	L (nm)	Lc (nm)	La (nm)
EVA	10.83	4.53	6.20
ZnO/EVA	11.42	4.42	7.00
POE	11.95	5.65	6.30
ZnO/POE	12.57	5.97	6.60
LLDPE	16.13	6.70	9.43
ZnO/LLDPE	16.57	6.90	9.67
HDPE	21.10	13.60	7.50
ZnO/HDPE	21.14	13.54	7.60

to the larger particle diameter and lower content of nano ZnO. According to Table 7, it can be observed that the Lc values of ZnO/POE and ZnO/LLDPE are increased compared to the pure materials. This is attributed to the early crystallization induced by nano ZnO, as discussed in the DSC section. However, the Lc value of ZnO/EVA is reduced compared to the pure material. Although nano ZnO also acts as a nucleating agent for EVA, the hydrophilicity of EVA makes it more susceptible to interaction, thereby inhibiting the crystallization of EVA. The Lc value of ZnO/HDPE is slightly decreased compared to HDPE. This can be attributed to the strong crystallization ability of HDPE, making it difficult for nano ZnO to promote its crystallization. Instead, nano ZnO acts as an impurity, slightly inhibiting the crystallization of HDPE.

On the other hand, Table 7 shows that HDPE has the largest long period (20.10 nm), which decreases in the order of

LLDPE (16.13 nm), POE (11.95 nm), and EVA (10.83 nm). This indicates that HDPE has the strongest barrier capacity compared to the other three polyolefins. As a result, nano ZnO particles are most difficult to migrate to the surface of HDPE, which corresponds to the low antibacterial ability of ZnO/HDPE (Table 5). It is noteworthy that the ratio of crystallinity to the long period in POE is significantly higher than that in LLDPE, indicating that POE has more closely packed crystals, resulting in a stronger barrier ability of POE to ZnO than LLDPE. This is also the reason why the antibacterial rate of ZnO/POE is lower than that of ZnO/LLDPE. This is also reflected in the oxygen (O_2) barrier capability.

Table 8 lists the permeance and permeability coefficient of POE and LLDPE. The permeance values for POE and LLDPE are 334.96 cm^3/(m^2·24 h·0.1 MPa) and 556.74 cm^3/(m^2·24 h·0.1 MPa), respectively, indicating that the volume of O_2 passing through POE per unit area is much smaller than that passing through LLDPE in 24 h. The significant difference in O_2 transmission between POE and LLDPE is due to the difference in film thickness. Therefore, to compare the barrier ability of the films to oxygen, the film thickness is normalized using the permeability coefficient value. As shown in Table 8, the permeability coefficients of POE and LLDPE membranes are almost the same, suggesting that there is little difference in the O_2 barrier capacity between POE and LLDPE. Generally, the higher the crystallinity, the greater the gas barrier capacity of the material [44]. Although POE and LLDPE have the same oxygen barrier capacity, the crystallinity of POE is lower than that of LLDPE, at 32.47% versus 38.01%. This further confirms that the crystals in POE are more closely packed than those in LLDPE.

Surface morphology of nano ZnO composites

Figure 5 displays the SEM images of five nano ZnO composite films magnified at 20,000 times. As shown in the figure, the particle size on the surfaces of LLDPE and EVA is relatively large, which is attributed to the aggregation of nano ZnO on the surface over time after migration [45]. However, EVA and LLDPE exhibit a higher density of surface particles, while POE has fewer surface particles. HDPE, on the other hand, shows a significantly sparse distribution of surface particles, and PC exhibits almost no noticeable particles. These differences can be attributed to the

varying ability of the substrates mentioned earlier to hinder the migration of nano ZnO to the surface. By considering Table 5, it becomes evident that a higher density of surface particles leads to better antibacterial effects, which aligns with the conclusions drawn in previous sections.

In conclusion, during processing, a large MI and excellent fluidity have a positive effect on the dispersion of nano ZnO, which is beneficial for improving the antibacterial rate. When the MI is similar, materials with higher crystallinity have a greater influence on the ability of nano ZnO to migrate out of the surface, thereby reducing the antibacterial rate of the composite. Additionally, PC with T_g significantly higher than room temperature also blocks the migration of nano ZnO, resulting in a reduction of the antibacterial rate of ZnO/PC. However, crystallinity is not the only factor that affects the migration of nano ZnO. A small and densely layered arrangement can also increase the difficulty of nano ZnO migration out of the surface, leading to a reduction in antibacterial performance.

Nano ZnO effect on spherical crystal morphology for different polymers

The size and morphology of spherulites were investigated by laser scattering, as shown in Fig. 6. The PC group did not exhibit "four-leaf clover" patterns, indicating the absence of spherulites in the PC and ZnO/PC. This can be attributed to the amorphous of its molecular chains, which makes it challenging for them to arrange themselves in an orderly manner and form spherulites. The four polyolefin groups all formed "four-leaf clover" patterns, indicating that these materials formed spherulites with different sizes and regularity. The spherulite size can be calculated using Eq. (2). As seen in Fig. 6, pure POE had the largest spherulite size (7.45 μm), followed by EVA, LLDPE, and HDPE, with corresponding sizes of 5.57 μm, 2.67 μm, and 1.89 μm. Among these, the edges of the spherulite pattern of EVA and LLDPE were clearer, and the "four-leaf clover" pattern was more perfect than that of HDPE and POE. The spherulite patterns of the four nano ZnO composites are also shown in Fig. 6(f, g, h, i). The spherulite patterns of the composites were larger and had blurrier edges compared to those of the four pure materials, indicating a lower regularity in the formation of spherulites within the composites. The spherulite perfection of ZnO/POE decreased most significantly, and the spherulite size decreased greatly. The spherulite perfection of ZnO/HDPE was also significantly reduced, and the spherulite size decreased from 1.89 μm to 1.50 μm. The spherulite perfection of ZnO/EVA and ZnO/LLDDPE did not decrease significantly, but the spherulite size of EVA decreased significantly (from 5.57 μm to 1.05 μm). This may be because nano ZnO acts as impurities in the crystallization process, affecting the perfection and size of spherulites.

Table 8 The permeance and the permeability coefficient of POE and LLDPE

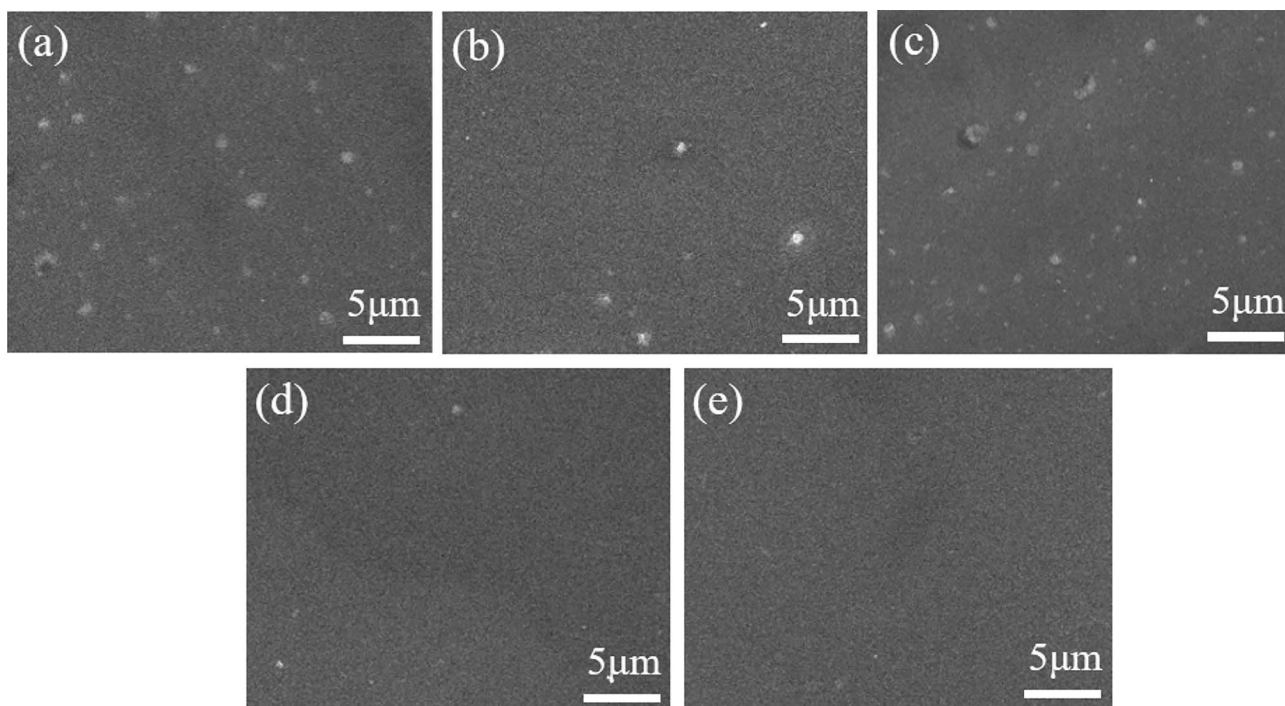| Sample	POE	LLDPE
film thickness (μm)	317	189
Permeance (cm^3/(m^2·24 h·0.1 MPa))	334.96	556.74
Permeability (cm^3·cm/cm^2·s·cmHg)	1.66×10^{-10}	1.65×10^{-10}

Fig. 5 SEM of (**a**) ZnO/EVA, (**b**) ZnO/POE, (**c**) ZnO/LLDPE, (**d**) ZnO/HDPE, (**e**) ZnO/PC

Nano ZnO effect on optical performance for different polymers

The internal haze of the film is a thickness-normalized value, and the measurement of surface haze is not affected by the film thickness. As shown in Table 9, PC has the lowest internal haze (0.04%) and better light transmittance (92.0%) because it is an amorphous polymer and almost non-crystalline, with no difference between refractive indexes. Therefore, polycarbonate has good transparency and low haze. As seen in Table 9, EVA and POE have lower haze at 4.71% and 0.87%, respectively, while
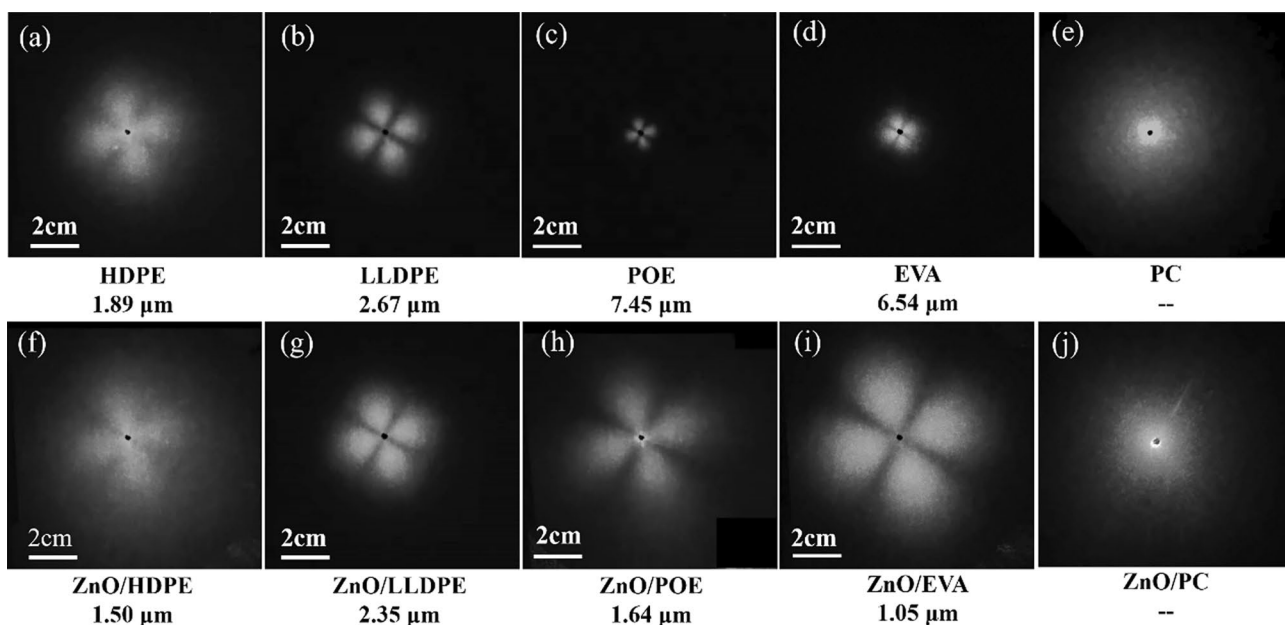

Fig. 6 Spherulite morphologies of (**a**) HDPE, (**b**) LLDPE, (**c**) POE, (**d**) EVA, (**e**) PC, (**f**) ZnO/HDPE, (**g**) ZnO/LLDPE, (**h**) ZnO/POE, (**i**) ZnO/EVA and (**j**) ZnO/PC

LLDPE and HDPE have higher haze at 13.34% and 10.69%, respectively. This is due to the difference in crystallinity (Table 6). Among them, the internal haze of EVA with lower crystallinity is higher than that of POE because the perfect spherulites of EVA increase light scattering compared to POE. The internal haze of HDPE, which has the highest crystallinity, is less than that of LLDPE, which is related to the imperfection of HDPE spherulites. In semi-crystalline polymers, the light transmittance of EVA and POE is 92.0% and 92.3%, respectively, followed by LLDPE and HDPE. POE introduces a long branch chain in the main chain to improve the material's transparency. DSC results show that HDPE has the highest crystallinity, resulting in the lowest light transmittance (88.1%). Compared to pure materials, the light transmittance of nano ZnO composites is reduced due to the addition of nano ZnO particles with a larger refractive index, leading to greater scattering loss and reduced light transmission of the films. The internal haze of ZnO/EVA, ZnO/LLDPE, and ZnO/PC is increased compared to that of pure materials because the 15 nm nanometer increases the internal defects of the film. In comparison, the internal haze of ZnO/POE and ZnO/HDPE decreases compared to pure materials, which may be due to the decrease in spherulite perfection.

Tear resistance of pure materials and corresponding nano ZnO composites

In this study, compressed films were made for right-angled tearing strength tests. As shown in Fig. 7, the tear strength of nano ZnO composite polyolefin films is stronger than that of corresponding pure polyolefin films, indicating that these composite films have better tear performance. This is because the inorganic nanoparticles produced stress concentration in the matrix, which could absorb energy,

Table 9 Haze and transmittance of pure materials and corresponding nano ZnO composites

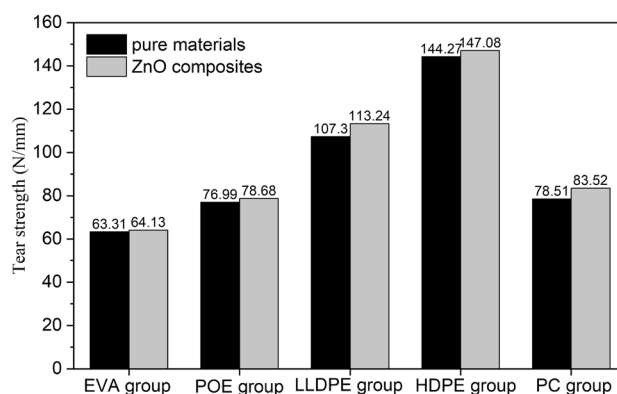| Sample	Normalized Internal Haze (%)	Transmittance (%)
EVA	4.71	92.0
ZnO/EVA	12.78	91.4
POE	0.87	92.3
ZnO/POE	0.76	91.4
LLDPE	13.34	90.4
ZnO/LLDPE	16.56	89.6
HDPE	10.69	88.1
ZnO/HDPE	8.22	87.7
PC	0.04	92.0
ZnO/PC	2.04	91.2

Fig. 7 Tear resistance of pure materials and corresponding nano ZnO composites

resulting in a good reinforcement effect. Among the pure polyolefins, HDPE has the largest tear resistance, with a tear strength of 144.27 N/mm. Similarly, the tear strength of PC and ZnO/PC are 78.51 N/mm and 83.52 N/mm, respectively. This is because HDPE has highly regular, closely arranged molecular chains and large lamellar spacing. The tear strength of LLDPE, with a slightly lower lamellar thickness than that of HDPE, is 107.30 N/mm. The tear strength of EVA and POE, which have smaller lamellar sizes, is 63.31 N/mm and 76.99 N/mm, respectively. This is because it is more difficult to slide and rotate the large-sized lamellae with regular arrangement.

Conclusions

In this study, excellent antibacterial activity (99.9%, R = 6.9) was obtained from nano ZnO composites prepared from different matrices, with a solid content of 0.2%. However, when the content of nano ZnO is reduced to 0.05%, the study of molecular chain fluidity, crystallinity, and crystal structure helps to illustrate why different matrices exhibit different antibacterial activities.

The EVA with a high melt index (MI) and strong fluidity is more conducive to the uniform dispersion of nano ZnO in the processing process, resulting in better antibacterial activity. The freezing of molecular chains (as in PC) at room temperature can also affect the migration of nano ZnO, leading to a reduced antibacterial rate (55.4%). Among the four semi-crystalline polymers, HDPE has the largest crystallinity, larger lamellar thickness, and stronger barrier ability, and therefore, the antibacterial ability of ZnO/HDPE (0.05%) is the lowest (46.4%). ZnO/LLDPE (0.05%) has the highest antibacterial rate (99.3%, R = 2.1), while the antibacterial rate of ZnO/POE (0.05%) is significantly reduced (67.9%). Even though the (X_c) of LLDPE is slightly higher than that of POE, its oxygen-blocking ability is lower due to the shorter long-period and densely-arranged lamellae compared to POE. Although the

crystallinity of EVA is very low, the antibacterial rate of EVA is lower than that of LLDPE (95.2% vs. 99.3%) because the polarity of EVA hinders the migration of nano ZnO by interacting easily with ZnO. The molecular chain fluidity, functional groups, crystallinity, crystal structure, and spherulite morphology of the matrix can affect the mobility of ZnO, and, thus the antibacterial rate.

In addition, nano ZnO induces the size of spherulites of polymers to decrease and the degree of perfection to decrease, which ultimately leads to the reduction of the transmittance of materials. Moreover, nano ZnO increases the tear resistance of the polymer. This contributes to the development of product diversity with high antibacterial, high transparency and tear resistance.

Data availability The data that support the findings of this study are available on request from the corresponding author.

Declarations

Conflicts of interests The authors declare no competing interests.

References

1. Abdali H, Ajji A (2015) Development of antibacterial structures and films using clove bud powder. Ind Crop Prod 72:214–219. https://doi.org/10.1016/j.indcrop.2014.09.050

2. Dobrucka R, Ankiel M (2018) Possible applications of metal nanoparticles in antimicrobial food packaging. J Food Safety 39:e12617. https://doi.org/10.1111/jfs.12617

3. Augustine R, Malik HN, Singhal DK, Mukherjee A, Malakar D, Kalarikkal N, Thomas S (2014) Electrospun polycaprolactone/ZnO nanocomposite membranes as biomaterials with antibacterial and cell adhesion properties. J Polym Res 21:347. https://doi.org/10.1007/s10965-013-0347-6

4. Laijun L, Yu Z, Chaojing L, Jiacheng C, Lu W (2020) Facile preparation PCL/modified nano ZnO organic-inorganic composite and its application in antibacterial materials. J Polym Res 27:28. https://doi.org/10.1007/s10965-020-02046-z

5. Shadpour M, Vajiheh B (2016) Nanocomposites based on biosafe nano ZnO and different polymeric matrixes for antibacterial, optical, thermal and mechanical applications. Eur Polym J 84:377–403. https://doi.org/10.1016/j.eurpolymj.2016.09.028

6. Roberto P, Giuliana G, Giovanni V, Marius M, Philippe D (2013) PLA-ZnO nanocomposite films: Water vapor barrier properties and specific end-use characteristics. Eur Polym J 49:3471–3482. https://doi.org/10.1016/j.eurpolymj.2013.08.005

7. Manaf O, Leya RR, Prasanth R, Mohamed AMN, Sujith A (2021) Maleic anhydride grafted acrylonitrile butadiene styrene (ABS)/zinc oxide nanocomposite: an anti-microbial material. J Polym Res 28:284. https://doi.org/10.1007/s10965-021-02632-9

8. Daniele V, Loredana T, Fulvia V, Antonella, Ivana C, Gaetana P, Giovanni V (2020) Antibacterial Al-doped ZnO coatings on PLA films. J Mater Sci 55:4830–4847. https://doi.org/10.1007/s10853-019-04311-z

9. Gorkem G, Aysun A, Birol E, Ufuk P (2018) Production of metal oxide containing antibacterial coated textile material and investigation of the mechanism of action. Fiber Polym 19:2548–2563. https://doi.org/10.1007/s12221-018-8306-9

10. Atanu N, Sohee L, Kwang-sun K (2020) Antibacterial potential of Ni-doped zinc oxide nanostructure: comparatively more effective against Gram-negative bacteria including multi-drug resistant strains. RSC Adv 10:1232–1242. https://doi.org/10.1039/C9RA09512H

11. Ge M, Xiaoxi L, Liangchao L, Ru, Donghua J, Yan D, Haifeng C (2014) Cu-doped zinc oxide and its polythiophene composites: Preparation and antibacterial properties. Chemosphere 100:146–151. https://doi.org/10.1016/j.chemosphere.2013.11.053

12. Yang L, Wen Z, Junfeng Ni, Yongsheng C (2012) Mechanism of photogenerated reactive oxygen species and correlation with the antibacterial properties of engineered metal-oxide nanoparticles. ACS Nano 6:5164–5173. https://doi.org/10.1021/nn300934k

13. Nagarajan P, Rajagopalan V (2008) Enhanced bioactivity of ZnO nanoparticles-an antimicrobial study. Sci Technol Adv Mat 9:035004. https://doi.org/10.1088/1468-6996/9/3/035004

14. Leigang M, Biming S, Nawrat S, Chaomin M, Kezhen Q (2017) Facile synthesis of hierarchical ZnO microstructures with enhanced photocatalytic activity. Mater Sci-poland 35:45–49

15. Buzuayehu A, Enyew Amare Z, Aschalew T (2020) A review on enhancing the antibacterial activity of ZnO: mechanisms and microscopic investigation. Nanoscale Res Lett 15:190. https://doi.org/10.1186/s11671-020-03418-6

16. Rajesh K, Ahmad U, Girish K, Hari SN (2017) Antimicrobial properties of ZnO nanomaterials: a review. Ceram Int 43:3940–3961. https://doi.org/10.1016/j.ceramint.2016.12.062

17. Lingling Z, Yunhong J, Yulong D, Malcolm P, David Y (2007) Investigation into the antibacterial behaviour of suspensions of ZnO nanoparticles (ZnO nanofluids). J Nanopart Res 9:479–489. https://doi.org/10.1007/s11051-006-9150-1

18. Tamar G, Benny P, Ofir H, Israel F, Ehud B, Shlomo M (2011) Synthesis and characterization of zinc/iron oxide composite nanoparticles and their antibacterial properties. Colloid Surf A 374:1–8. https://doi.org/10.1016/j.colsurfa.2010.10.015

19. Olesja B, Katre J, Angela I, Kaja K, Monika M, Anne K (2013) Toxicity of Ag, CuO and ZnO nanoparticles to selected environmentally relevant test organisms and mammalian cells in vitro: a critical review. Arch Toxicol 87:1181–1200. https://doi.org/10.1007/s00204-013-1079-4

20. Abdel-Halim ES, Al-Deyab SS (2014) Antimicrobial activity of silver/starch/polyacrylamide nanocomposite. Int J Biol Macromol 68:33–38. https://doi.org/10.1016/j.ijbiomac.2014.04.025

21. Sharma RK, Balani K (2014) Mechanics of ZnO micro-rod and ZnO nanoparticle reinforcement in ultra-high molecular weight polyethylene biocomposite. J Phys D Appl Phys 47:345301. http://iopscience.iop.org/0022-3727/47/34/345301

22. Li SC, Li YN (2010) Mechanical and antibacterial properties of modified nano-ZnO/high-density polyethylene composite films with a low doped content of nano-ZnO. J Appl Polym Sci 116:2965–2969. https://doi.org/10.1002/app.31802

23. Negi H, Agarwal T, Goel ZR (2012) Comparative antibacterial efficacy of metal oxide nanoparticles against Gram negative bacteria. Ann Microbiol 62:765–772

24. Guinault A, Sollogoub C, Domenek S, Grandmontagne A, Ducruet V (2010) Influence of crystallinity on gas barrier and mechanical properties of PLA food packaging films. Int J Mater Form 3:603–606. https://doi.org/10.1007/s12289-010-0842-9

25. Rubino M, Netramai S (2010) Effect of Chlorine Dioxide Gas on Physical, Thermal, Mechanical, and Barrier Properties of polymeric packaging materials. J Appl Polym Sci 115:1742–1750. https://doi.org/10.1002/app.31244

26. Chowdhury SR, Sabharwal S (2011) Molecular-scale design of a high performance organic-inorganic hybrid with the help of gamma radiation. J Mater Chem 21:6999–7006. https://doi.org/10.1039/C1JM10943J

27. Hong-Biao C, Chang-Ying H (2018) Influence of PP types on migration of zinc from nano-ZnO/PP composite films. Packag Technol Sci 31:747–753. https://doi.org/10.1002/pts.2411

28. Alojz Anžlovar A, Primožič M, Švab I, Leitgeb M, Knez Ž, Žagar E (2019) Polyolefin/ZnO composites prepared by Melt Processing. Molecules 24:2432. https://doi.org/10.3390/molecules24132432

29. Guillaume D, Ibon A, Lorena G, Evgeni I, Ekaterina D, Rumania K, Marc V, Jeannette D (2014) Thermal and rheological characterization of antibacterial nanocomposites: poly(amide) 6 and low-density poly(ethylene) filled with zinc oxide. J Thermoplast Compos 27:268–284. https://doi.org/10.1177/0892705712445037

30. Chengcheng T, Yang L, Ying W, Xinlu H, Li-Zhi L (2023) Effect of polyethylene internal structure on antibacterial properties of nano silver composites. J APPL POLYM SCI 140:e53706. https://doi.org/10.1002/app.53706

31. Shujun W, Changjiang W, Min-Qiao R, Ryan MV, Matthew J, Erqiang CCH, Stephen C (2009) Liquid-liquid phase separation in a polyethylene blend monitored by crystallization kinetics and crystal-decorated phase morphologies. Polymer 50:1025–1033. https://doi.org/10.1016/j.polymer.2008.12.028

32. Xinlu H, Ying S, Li-Zhi L, Yi R, Yuanxia W (2021) Crystallization, structure, morphology, and properties of linear low-density polyethylene blends made with different comonomers. POLYM ENG SCI 61:2406–2415. https://doi.org/10.1002/pen.25766

33. Mylonas E, Svergun DI (2007) Accuracy of molecular mass determination of proteins in solution by small-angle X-ray scattering. J Appl Crystallogr 40:s245–s249. https://doi.org/10.1107/S002188980700252X

34. Mohand C, Françoise E, Isabelle M, Françoise B, Maria-Rosa A, María-Luisa LD, Julio SR, Nimet B, Erhan P, Omar Z, Roger C (2010) SAXS Investigation of the Effect of temperature on the Multiscale structure of a Macroporous Poly(N-isopropylacrylamide) gel. Macromolecules 43:2009–2017. https://doi.org/10.1021/ma902655h

35. Sedlak SM, Bruetzel LK, Lipfert J (2017) Quantitative evaluation of statistical errors in small angle X-ray scattering measurements. J APPL CRYSTALLOGR 50:621–630. https://doi.org/10.1107/S1600576717003077

36. Jellinek MH, Soloman E, Fankuchen I (1946) Measurement and analysis of small-angle X-ray scattering. Ind Eng Chem Anal Ed 18:172–175. https://doi.org/10.1021/i560151a005

37. Shu-Gui Y, Zhen-Zhen W, Liliana C, Pantea K, Xiang-bing Z, Hui-Jie X, Hina S, Goran U (2021) Bowls, vases and goblets-the microcrockery of polymer and nanocomposite morphology revealed by two-photon optical tomography. Nat Commun 12:5054. https://doi.org/10.1038/s41467-021-25297-w

38. Shi Y, Zheng C, Minqiao R, Yujing T, Li-Zhi L, Bob H (2017) Evaluation of principal residual stress and its relationship with crystal orientation and mechanical properties of polypropylene films. Polymer 123:137–143. https://doi.org/10.1016/j.polymer.2017.07.006

39. Enikő F (1993) Transport of small molecules in polyolefins. II. Diffusion and solubility of irganox 1076 in ethylene polymers. J Appl Polym Sci 48:1905–1913. https://doi.org/10.1002/app.1993.070481104

40. Jeevananda T, Siddaramaiah (2001) Thermal and morphological studies on ethylene-vinyl acetate copolymer–polyaniline blends. THERMOCHIM ACTA 376:51–61. https://doi.org/10.1016/S0040-6031(01)00530-5

41. Pavlicevic J, Spirkova M, Bera O, Jovicic M, Pilic B, Balos S, Budinski-Simendic J (2014) The influence of ZnO nanoparticles on thermal and mechanical behavior of polycarbonate-based polyurethane composites. COMPOS PART B-ENG 60:673–679. https://doi.org/10.1016/j.compositesb.2014.01.016

42. Shoichiro Y, Kimio K, Keisuke I, Takeshi F, Mitsuo K (2003) Structure and properties of poly(vinyl alcohol)/tungsten trioxide hybrids. Polymer 44:3515–3522. https://doi.org/10.1016/S0032-3861(03)00281-7

43. Li-Zhi L, Benjamin C, Benjamin C, Penning, JP, St. JR (1997) A Synchrotron SAXS Study of Miscible Blends of Semicrystalline Poly(vinylidene fluoride) and Semicrystalline Poly (1,4-butylene adipate). Macromolecules 30:4398–4404. https://doi.org/10.1021/ma961719n

44. Li Y, Wu XJ, Wen JG, Takahashi Y (2000) Dependence of crystallinity on oxygen pressure and growth mode of La. thin films on different substrates J Appl Phys 87:3707–3710. https://doi.org/10.1063/1.372404

45. Jian L, Yueqiang L, Baogang Z (2002) Spontaneous agglomeration of silver nanoparticles deposited on carbon film surface. J Nanopart Res 4:345–349. https://doi.org/10.1023/A:1021120723498